International Journal of Mass Spectrometry 311 (2012) 64–71

Contents lists available at SciVerse ScienceDirect

International Journal of Mass Spectrometry

journal homepage: www.elsevier.com/locate/ijms

Trapping charged nanoparticles in the nano aerosol mass spectrometer (NAMS)

M. Ross Pennington, Murray V. Johnston*

Department of Chemistry and Biochemistry, University of Delaware, Newark, DE 19716, United States

ARTICLE INFO

Article history:
Received 6 July 2011
Received in revised form
19 December 2011
Accepted 19 December 2011
Available online 27 December 2011

Keywords:
Quadrupole ion trap
Particle trapping
Particle mass spectrometer
Instrumentation
SIMION

ABSTRACT

Particle trapping in the nano aerosol mass spectrometer (NAMS) is investigated through a combination of modeling and experimental measurements to understand and optimize the trapping process. In the NAMS, charged nanoparticles pass through an aerodynamic lens, digital ion guide (DIG) and field adjusting lens (FAL) prior to entering a digital ion trap (DIT) where they are captured and subsequently analyzed. The DIT is operated with a square wave potential applied to the ring electrode. SIMION modeling was used to study particle motion from the exit aperture of the DIG into the DIT. Several parameters were characterized including particle starting position, kinetic energy, trajectory and FAL design. A new FAL assembly was designed to increase the number of trapped particles. The new design was found to increase the rate that ambient particles are analyzed by over an order of magnitude. With the new design, an ambient aerosol concentration ($dN/d\log d_m$) of 1×10^3 cm^{-3} yields approximately 2–3 particles analyzed per minute.

1. Introduction

Particles between about 1 and 50 nm in diameter (referred to as nanoparticles herein) are an important subset of ambient aerosol that have significant climate [1,2] and human health [3–5] impacts. Chemical composition measurements of ambient nanoparticles can assist research in these areas by providing insight into the sources and transformations of these particles in the atmosphere [6,7]. From a chemical analysis perspective, this is a difficult task because of the small amount of material involved. For example, a 25 nm unit density particle has a mass of about 8 attograms (8×10^{-18} g).

We have developed a nano aerosol mass spectrometer (NAMS) [8,9] to sample and analyze individual, singly charged 10–30 nm dia. particles from atmospheric pressure [10–12]. Chemical analysis is performed by irradiating individual particles with a tightly focused, high energy laser pulse. The laser radiation produces a plasma that reaches the complete ionization limit, where the particle is completely disintegrated into positively charged atomic ions [13]. The method of sampling nanoparticles into this instrument must meet two objectives. First, particles must be efficiently transmitted from atmospheric pressure into the vacuum. Second, particles must be spatially constrained within the focal region of the laser beam, preferably in a manner that can be used for size-selection. To accomplish the first objective, particles are transmitted from atmospheric pressure into the vacuum through a combination of aerodynamic and electrodynamic focusing elements. To accomplish the second objective, an electrostatic lens assembly is used to inject particles into an ion trap in a manner that maximizes trapping [8]. The complete instrument employs (in order of particle transit and analysis) an aerodynamic lens, a digital ion guide (DIG), a field adjusting lens (FAL), a digital ion trap (DIT), and a Nd:YAG laser along with time-of-flight mass analyzer for creating and analyzing atomic ions.

In order to maximize the rate at which particles are trapped and analyzed by NAMS, a fundamental understanding is needed of the trapping process and how the instrument design affects it, especially as a function of particle size. In this work, SIMION® is employed to model nanoparticle trapping. SIMION has been used in many studies to model ion trapping in conventional mass spectrometers [14–17] and to model low m/z ions in a digital ion trap (DIT) [18]. We apply the knowledge gained to the design, implementation and demonstration of an improved configuration for NAMS for the trapping and subsequent mass spectrometric analysis of nanoparticles.

2. Experimental

2.1. Experimental measurements with NAMS

A schematic of the NAMS is shown in Fig. 1. From right to left (direction of charged particle and atomic ion motion as indicated in the figure), the instrument consists of an aerodynamic lens inlet, a digital ion guide (DIG), a digital ion trap (DIT), and a reflectron time-of-flight (TOF) mass analyzer. A full description of the NAMS is given elsewhere [9]. Below, we describe only those aspects of the instrument that relate directly to this study.

* Corresponding author. Tel.: +1 302 81 8014; fax: +1 302 831 6335.
E-mail address: mvj@udel.edu (M.V. Johnston).

1387-3806/$ – see front matter © 2011 Elsevier B.V. All rights reserved.
doi:10.1016/j.ijms.2011.12.011

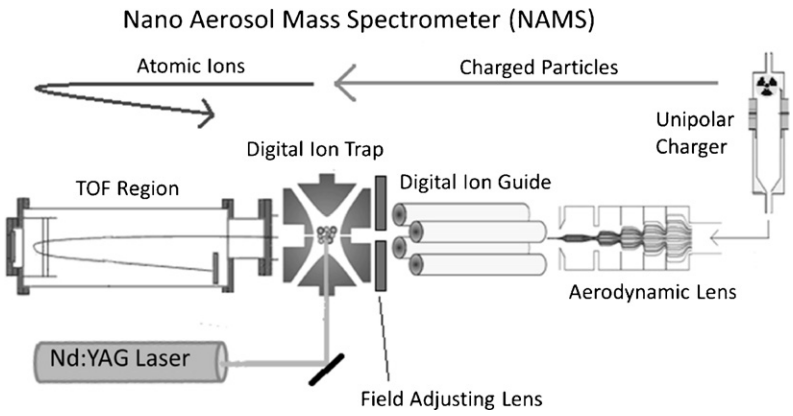

Fig. 1. A schematic of the nano aerosol mass spectrometer (NAMS) with the "old" FAL design.

Test aerosols used in this study were generated with an Electrospray Aerosol Generator (model 3480, TSI Inc., Minnesota). This unit electrosprays analyte solutions (typically 0.2%, w/w, in 0.02 M ammonium acetate buffer) in the presence of a radioactive source to neutralize the primary droplets and minimize Raleigh breakup as the solvent evaporates. This results in an aerosol whose size distribution can be adjusted within the 10–30 nm size range (size distribution depends primarily on the analyte concentration of the electrosprayed solution), and each particle has either zero or one charge. The aerosol is sent through a unipolar charger [19] which increases the fraction of particles having a single positive charge [20]. The particle size distribution is monitored and specific particle sizes are selected for experiments requiring a monodisperse distribution with a Scanning Mobility Particle Sizer (SMPS; Electrostatic Classifier, model 3080, Condensation Particle Counter, model 3025a, TSI, Inc., St. Paul, Minnesota), which also helps pull the aerosol through the unipolar charger to the NAMS inlet. With the SMPS, particle size is measured and/or selected on the basis of mobility diameter (d_m).

Instrument performance was also assessed through ambient aerosol measurements. Data are presented for two measurement campaigns: Pasadena, California in May–June 2010 using the "old" NAMS design (128,761 ambient particles analyzed); Hyytiälä, Finland in March–April 2011 using the "new" NAMS design (93,951 ambient particles analyzed).

Aerosol passing across the NAMS inlet is sampled through a 0.1-mm-dia. flow limiting orifice into the aerodynamic lens similar to the design of Wang et al. [8], which is maintained at a sub-ambient pressure of 1.5 torr. Particles exiting the lens traverse a ~6-mm field-free, differentially pumped region and pass through a 1-mm-dia. entrance aperture to the DIG. The DIG consists of four cylindrical rods with square wave potentials applied to them. The rods are configured similar to a quadrupole ion guide, that is the two opposing rods have a waveform that is 180° phase-shifted from the other two. The frequency of the square wave potential is fixed at 50 kHz with amplitudes of −500/+500 V. The dynamic electric field produced by these rods is sufficient to focus singly charged particles in the targeted size range of 10–30 nm dia. toward the centerline of the DIG. Particles exit the DIG through a 1-mm-dia. aperture that permits differential pumping. Argon gas is leaked into the DIG to collisionally cool the particles as they traverse this region, both to assist the focusing effect of the DIG and to increase the probability of trapping further downstream in the DIT. As discussed later, particles exiting the aerodynamic lens are much too energetic to be efficiently trapped, and must be translationally cooled prior to entering the DIT. As particles exit the DIG, they pass through the so-called field adjusting lens (FAL) [18]. This lens is slightly different in form and function than that described by Ding et al. [18] for a conventional DIT mass spectrometer. For the NAMS, this lens serves to manipulate the particle trajectory into the DIT.

The DIT consists of two end caps and a ring electrode in a configuration similar to that of a conventional quadrupole ion trap (r_0 = 10 mm, z_0 = 7.1 mm). A square wave potential is continuously applied to the ring electrode, which operates at an amplitude of −507 V/+504 V with a variable frequency based on the particle size being analyzed. In the work presented here, a frequency of 10 kHz is used. As discussed previously, the DIT traps particles over a size range based on the mass normalized diameter (d_{mn}), which is defined as the diameter of a spherical particle with unit density that has the same mass as the particle being trapped. Eq. (1) shows the relationship between the mobility diameter (d_m) and mass normalized diameter (d_{mn}) for spherical particles:

$$d_{mn} = d_m \left(\frac{\rho}{\rho_0} \right)^{1/3} \quad (1)$$

where d_m is the mobility diameter, d_{mn} is the mass normalized diameter, ρ is the particle density and the reference density is assumed to be 1 g/cm^3.

A pulsed valve attached directly to the DIT supplies argon gas to this region in a manner that maximizes the DIT pressure during the trapping period while maintaining an average pressure of ~1–3 × 10^{-4} mbar in the differentially pumped chamber surrounding the DIT. Argon collisionally cools the particles to increase the probability of trapping and to focus them to the center of the DIT. Particle trapping occurs over a 250 ms time period. At the end of this period, a Nd:YAG laser (model CFR400, Big Sky Lasers, Billings, Montana) operating at ~200 mJ/pulse, is fired and the laser radiation is tightly focused to the center of the DIT. The laser radiation interacts with the trapped particle to form a plasma that disintegrates the particle into positively charged atomic ions. Immediately before the laser fires, the end caps are pulsed to +1300 V and −500 V (front to back in the direction of particle and ion motion inside the DIT) to extract the atomic ions into the TOF drift tube (R. M. Jordan Co., Inc., Grass Valley, California). The ion extraction period is timed to coincide with the +504 V portion of the square wave potential applied to the ring electrode.

2.2. Modeling particle motion through the NAMS

In this study, particle motion from the exit aperture of the DIG through the FAL and into the DIT is explicitly modeled. Particle motion through the aerodynamic lens and DIG is not modeled. Instead, the net effect of these components is incorporated into the model through the selection of starting conditions for particles leaving the exit aperture of the DIG. The range of starting

conditions is sufficiently broad that it encompasses all likely values for particles exiting the DIG.

A model built with SIMION® (Scientific Instrument Services, Inc., Ringoes, New Jersey) is summarized in Fig. 2a, which includes the DIT (electrodes I, II, and III), the FAL electrode (IV), and exit aperture from the DIG (V). The dimensions of the model in Fig. 2a match what we will refer to as the "old" design of the NAMS reported previously. Fig. 2b shows a different ("new") design that will be discussed later. User programs were employed to apply a square wave potential to the ring electrode (II in Fig. 2a) and adjustable, static potentials to the other electrodes. The exit aperture from the DIG (V in Fig. 2a) was held at ground. The program also modeled collisional cooling throughout the simulation using the hard sphere method developed by Manura [21]. This model utilizes the mean free path to calculate a collision probability and then to randomize the collision factor, which is a number from 1 to 0, 1 being a direct hit and 0 being a "rear-end" collision. This model is expected to be more accurate at the (low) pressure of our DIT than the viscous cooling method. For all simulations, the argon pressure was assumed to be 1×10^{-3} mbar inside the DIT and 1×10^{-4} mbar outside the DIT. These pressures are based on the average pressure measured outside the DIT and the expected pressure inside the trap is based on conductance calculations. The pressures do not take into account the pulsed nature of the argon flow, which is impossible to simulate accurately.

For all simulations, unless otherwise noted, 10^6 25 nm particles started at the DIG exit aperture with initial conditions that were systematically varied: particle starting position, angular trajectory with respect to the *Z*-axis (centerline of the trap assembly), initial kinetic energy, time of birth, trap frequency and pressure. The time of birth (TOB) is used to model the "phase" of the ring electrode potential that the particle experiences when it enters into the trap assembly. The beginning of the positive cycle of the ring electrode potential corresponds to a TOB = 0. In order for a particle to be considered trapped it must have a lifetime of over 10 ms in the DIT, that is to say it must not leave the simulation region or strike an electrode. While this time period is smaller than the full trapping period of the NAMS (250 ms), it is long enough to distinguish particles with low kinetic energies (low velocities) within the assembly that are not trapped from particles that appear to be captured within the DIT. Each simulation was performed in triplicate.

3. Results and discussion

Particles entering the NAMS are carried from atmospheric pressure into the partial vacuum of the aerodynamic lens. The pressure differential across the flow limiting orifice has the effect of accelerating particles into the lens assembly. A relaxation chamber at the beginning of the lens assembly allows the particles to collide with gas molecules to reduce their velocities back to a thermal distribution, while the remaining lens elements focus particles toward the centerline of the aerosol flow. A similar acceleration occurs as particles exit the lens assembly toward the digital ion guide (DIG). The purpose of the DIG is two-fold. First, collisions between particles and argon atoms in the DIG decrease the particle velocities toward a thermal distribution. Second, the electric field within the DIG serves to focus (charged) particles toward the centerline of the aerosol flow.

Wang et al. [22,23] have estimated the mean velocities (and kinetic energies) of nanoparticles exiting an aerodynamic lens assembly similar to ours. The kinetic energies are particle size dependent, with larger particles acquiring larger kinetic energies. The kinetic energies determined by Wang et al. are used as the starting point for our simulations. Mean free path calculations allow determination of the amount of translational cooling that these particles experience as they transit through the DIG. When combined with the initial kinetic energies of Wang et al., they provide an estimate of the kinetic energies of particles exiting the DIG aperture (electrode V in Fig. 2a). The calculated kinetic energies range from 8 eV for 10 nm particles to 440 eV for 25 nm particles. While these estimates are helpful, they are not accurate because particle motion is complex inside the aerodynamic lens and DIG. Therefore, the simulations below were performed with particle kinetic energies up to 1000 eV which was considered more than adequate to encompass the entire distribution of energies.

Particles entering the DIT experience a decelerating potential caused by the positive cycle of the ring electrode potential. The electric field experienced by the particles is fine-tuned by the FAL voltage to maximize the probability of particle trapping. The FAL (electrode IV in Fig. 2a) is an essential portion of the NAMS which enables the trapping of large particles. Without this electrode, particles would not be trapped. In the NAMS, the FAL primarily acts as an Einzel lens and serves to focus particles as they enter into the DIT, giving them an acceptable trajectory for trapping. The stability criterion for trapping ions (or in our case charged particles) in a DIT has been discussed by Ding et al. [18]. Charged particles can adopt stable trajectories in the trap when $q_z \leq 0.712$:

$$q_z = \frac{4\,\mathrm{eV}}{mr_o^2(2\pi f)^2} \leq 0.712 \tag{2}$$

where r_o is the trap radius, V and f are the amplitude and frequency of the square wave potential applied to the ring electrode, m is the mass of the particle and e is the charge of the particle. Eq. (2) gives the lower particle size limit for trapping. For example, for a trap frequency of 10 kHz, the small particle size (d_{mn}) cutoff for trapping is approximately 16 nm, because at this size $q_z \approx 0.7$. Eq. (2) shows that q_z decreases as the particle size increases, implying that infinitely large particles can be trapped. However, the pseudo-potential well depth that is created within the trap must be taken into account. For a DIT, the pseudo-potential well depth (D_z) is given by

$$D_z \approx 0.206(q_z V) \tag{3}$$

where q_z and V are defined above. As the particle size increases and q_z decreases, there comes a point where the particle can no longer be trapped because its kinetic energy exceeds the potential well depth. The largest kinetic energy of a charged particle that can be trapped is given by [24]

$$\mathrm{KE} = \frac{1}{2}mv^2 < D_z + E_{\mathrm{cooling}} \tag{4}$$

where KE is the kinetic energy of a particle entering the DIT and E_{cooling} is the amount of energy the particle loses inside the DIT through collisions with argon gas. Note that KE increases and E_{cooling} decreases as the particle size increases. Eqs. (2) and (4) define the effective particle size range that can be trapped. If the particle is too small, it does not meet the stability criterion of Eq. (2). If the particle is too large, it does not meet the kinetic energy criterion of Eq. (4).

Fig. 3a shows the values of q_z and D_z vs. mass normalized diameter (d_{mn}) for a 10 kHz trap frequency. The shaded area is the approximate size range where particles have been shown experimentally to be analyzed by NAMS when using a ring electrode potential of −507 V/+504 V and a frequency of 10 kHz. The minimum D_z in Fig. 3a roughly matches the KE of particles that can be trapped.

3.1. Particle trapping simulations

Fig. 3a shows that it is *possible* to trap particles over a specific size range (d_{mn}). This size range can be shifted to higher or lower d_{mn} by decreasing or increasing the frequency of the square wave

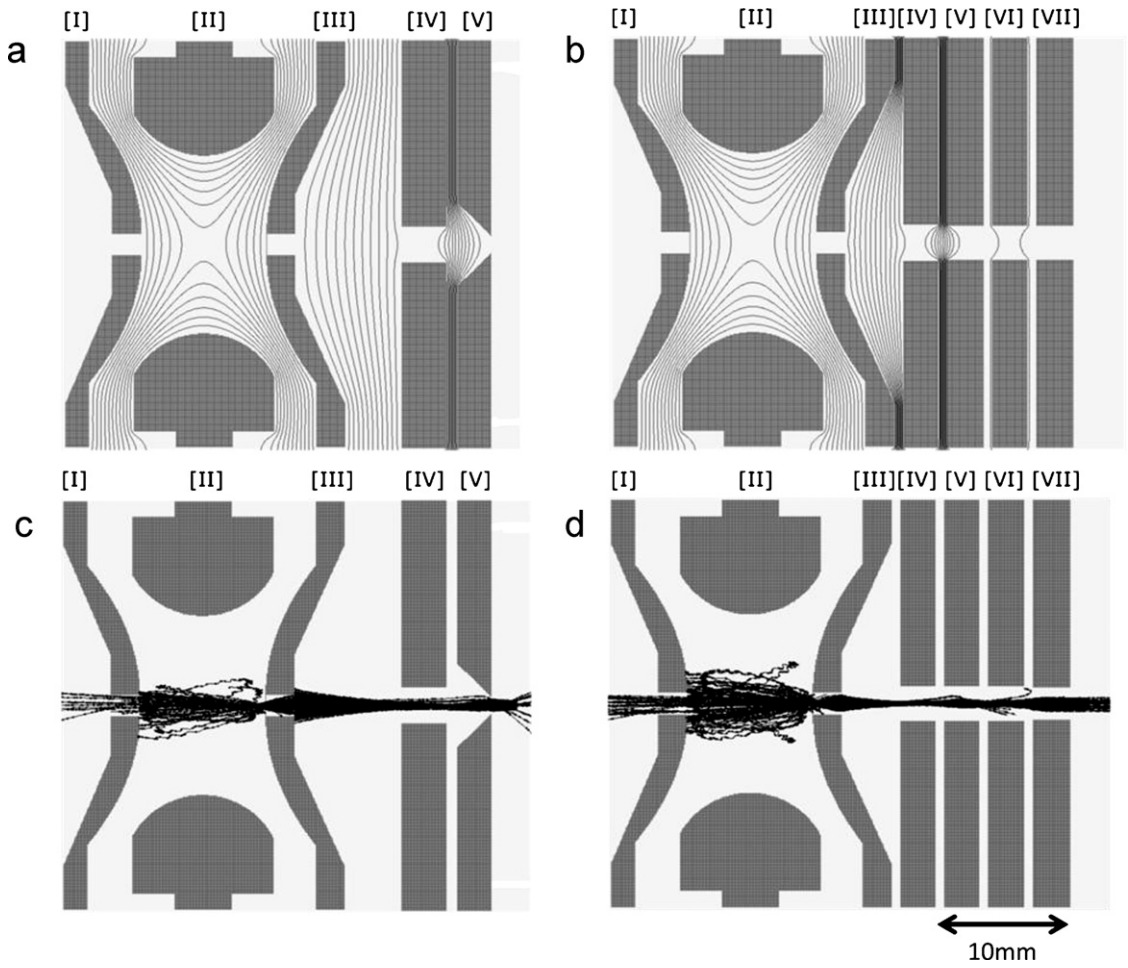

Fig. 2. SIMION models for (a) the old design and (b) the new design of the FAL. In each design, I, II and III represent the end caps and ring electrode of the DIT; IV represents the FAL; and the electrode to the far right represents the exit aperture from the DIG. Field lines show ~42 V increments for 0 V applied to the DIG exit aperture, −500 V applied to the FAL, −2 V applied to the DIT end caps and −500 V applied to the DIT ring electrode. Trajectories for 200 representative particles showing focusing and loss characteristics of the old (c) and new (d) designs.

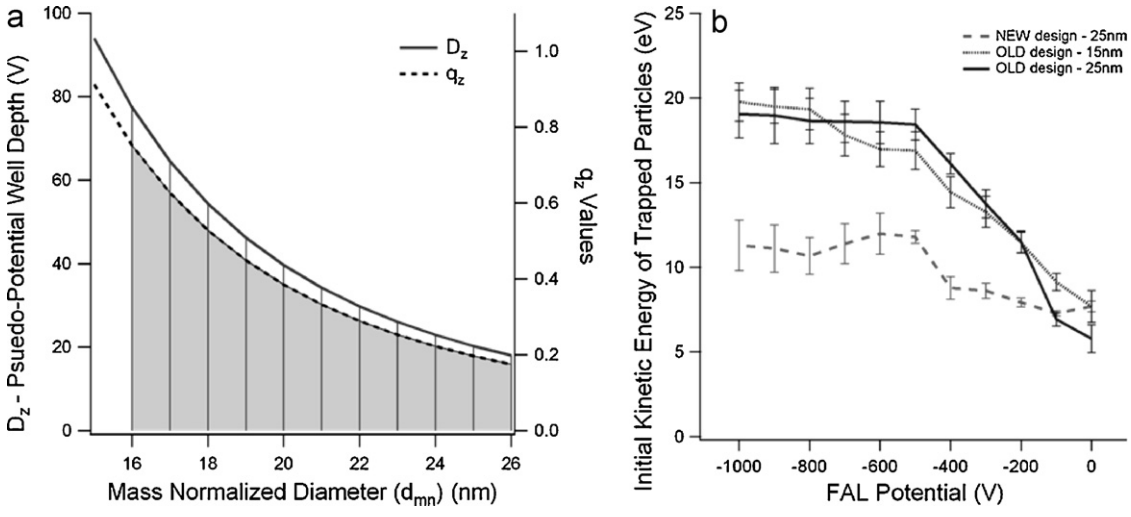

Fig. 3. (a) D_z and q_z vs. particle size for the DIT in the NAMS. The shaded region represents the approximate size range of particles that can be trapped with a DIT ring electrode potential of −507 V/+504 V and frequency of 10 kHz. (b) Kinetic energy vs. FAL potential for 25 and 15 nm dia. trapped particles (old design) and 25 nm dia. particles (new design). Ring electrode frequencies are 10 and 13 kHz respectively for 25 and 15 nm dia. particles.

applied to the ring electrode. Whether or not particle trapping is *probable* depends on the characteristics of particles exiting the DIG. The parameters investigated include the initial kinetic energy (KE), position, trajectory, and time of birth (TOB). Each of these is discussed below.

3.1.1. Initial particle kinetic energy

As particles exit the aerodynamic lens they are imparted a KE that is based in their mass. When they subsequently traverse the DIG they are cooled by the argon bath gas. Mean free path calculations were used to estimate the KE of particles exiting the guide in both the old and new designs. Because of the inaccuracy of these calculations, these values of particle kinetic energy were NOT used in subsequent modeling. However, the values calculated using MFP calculations illustrate two general concepts: (1) kinetic energy increases with particle size due to the decreased amount of collision cooling received in the guide and (2) particles can have a wide range of kinetic energies as they exit the guide. Instead of restricting particle energies to those calculated, simulations of particle motion after the DIG were performed by varying the particle initial kinetic energy over a very wide range from 0 to 1000 eV to encompass a much wider range than suggested by MFP calculations.

The field adjusting lens (FAL) potential was varied from 0 to −1000 V to determine its relationship to particle kinetic energy and the probability of trapping. As shown in Fig. 3b, there is a strong relationship among the three. For a given initial kinetic energy, a specific FAL voltage is required for trapping. Simulations for 15 and 25 nm (d_{mn}) particles (Fig. 3b, old design) show that the FAL voltage required for trapping is the same for both particle sizes for a given kinetic energy. In this regard, the FAL voltage can be considered independent of particle size. However, different particle sizes have different initial kinetic energies, so in practice a different FAL voltage is required for each particle size. The observation that the FAL voltage depends only on kinetic energy suggests that its main effect is to modify where particles are focused in the DIT so that they can be trapped. This effect is illustrated in Fig. 2c where a subset of the particle trajectories is shown (200 out of 10^6 particles). The subset of particles in Fig. 2c and d has the same range of starting conditions as described in Section 2 (KE, starting position, trajectory) and the FAL voltage was −500 V. It is clear that particles are focused by the FAL potential as they transit this region. Given that the FAL seems to act much like an Einzel lens (Fig. 2c) and we assume that there is an ideal focal point for a given d_{mn}, this focal point will be dependent on particle kinetic energy and FAL potential. While Fig. 3a suggests that particles can be trapped inside the DIT over a wide range of sizes, the FAL dependence in Fig. 3b suggests that in practice the size range will be narrowed owing to the manner in which particles are injected into the DIT.

3.1.2. Initial particle position and trajectory

The particle starting position for the "old" design in Fig. 2a is limited by the 1 mm dia. exit aperture from the DIG. Simulations were performed by constraining the initial starting position to a random circular distribution with a 0.5 mm radius from the *Z*-axis (centerline of particle motion). For all simulations particles were started at the same position along the *Z*-axis, at a point well outside the simulation. "Starting position" defines each particle's position in the *x*–*y* plane. The starting trajectory was allowed to vary in a cone distribution, also around the *Z*-axis with an angle up to 10°. Together these variables illustrate how particle focusing in the DIG may influence trapping further downstream. Varying these parameters in the simulation had a substantial effect on particle trapping in the DIT. Fig. 4a details how the starting particle position determines whether the particle is trapped. For these simulations, particles are given the representative range of energies (0 to −1000 V), starting position and TOB (discussed in Section 3.1.3). A DIT potential and frequency of 507 V/+504 V and 10 kHz, respectively, and a FAL potential of −500 V were used. Shown in Fig. 4 are all trapped particles from this simulation. Particles cannot have starting positions that are very close to or very far away from the *Z*-axis. Furthermore, particles cannot have very large (greater than 7°) or small (less than 1°) diverging angles. Only particles having intermediate starting positions and diverging angles are trapped. These results also highlight the crucial role that the FAL plays in particle trapping – without it, hardly any particles exiting the DIT aperture would have particle trajectories that permit trapping. For the remainder of these simulations, particle trajectory was confined to having diverging angles less than 7°, while particle starting position was allowed to have the same range (circular distribution with a radius of 0.5 mm).

3.1.3. Particle time of birth (TOB)

The time at which a particle enters the DIT relative to the phase of the ring electrode potential is another important consideration. For this simulation, the particle TOB was allowed to vary from 1 to 150 μs, which encompassed 1.5 cycles of the ring electrode potential. The particle size was 25 nm, the ring electrode potential and frequency were −507 V/+504 V and 10 kHz, respectively, and the FAL voltage was −500 V. Fig. 5a shows the kinetic energies of particles that were trapped as a function of TOB for the "old" design. (A similar plot is shown in Fig. 5b for the "new" design that will be discussed later). Superimposed in Fig. 5a is the ring electrode potential at the time each particle emerges from the DIG aperture. While trapping is possible only over a narrow range of kinetic energies, a clear relationship exists within this range between particle kinetic energy and TOB. If a particle exits the DIG at the beginning of the positive portion of the trap cycle, it is decelerated slightly less than particles exiting the DIG later in the cycle. Interestingly, an overlap in the region near the beginning/end of the trap cycle exists where particles can have one of two distinct kinetic energies and still be trapped. The dependence in Fig. 5a represents a combination of several factors including the potential barrier at the entrance of the DIT caused by the positive cycle of the ring voltage, modification of the potential barrier by the FAL voltage, and particle motion into and within the DIT as the ring voltage changes polarity.

The plots in Figs. 4 and 5 have several implications for operation of the NAMS. First, the particle kinetic energy must be matched with the FAL potential. Second, for a given particle size, the distribution of kinetic energies leaving the DIG must be narrow. Otherwise a single FAL voltage will not allow all particles to be trapped. Third, the entire trap cycle may not be available for particle trapping since the kinetic energy required changes with time point in the cycle.

3.2. A new trap assembly for NAMS

The SIMION model provided the opportunity to test other FAL designs that could be incorporated into the existing instrument. Several configurations were explored, and the one found to be most promising is shown in Fig. 2b. The FAL in this design (electrode IV) is only 2.5 mm wide (down from 5 mm) and abutted against the trap end cap of the DIT. An Einzel lens assembly is inserted between the FAL and the DIG (electrodes V–VII). This design also includes a larger DIG exit aperture diameter (2 mm).

3.2.1. Simulations with the new design

Simulations were performed with the new FAL design using the same particle starting positions, trajectories and range of kinetic energies as before. The Einzel lens was held at −25 V and the FAL voltage was varied and its effect on particle trapping was determined. As shown in Fig. 3b, the kinetic energies of trapped particles with the new design are much lower for a given FAL voltage than with the old design. Furthermore, Fig. 5b shows that the kinetic energies of trapped particles are allowed to have a larger range

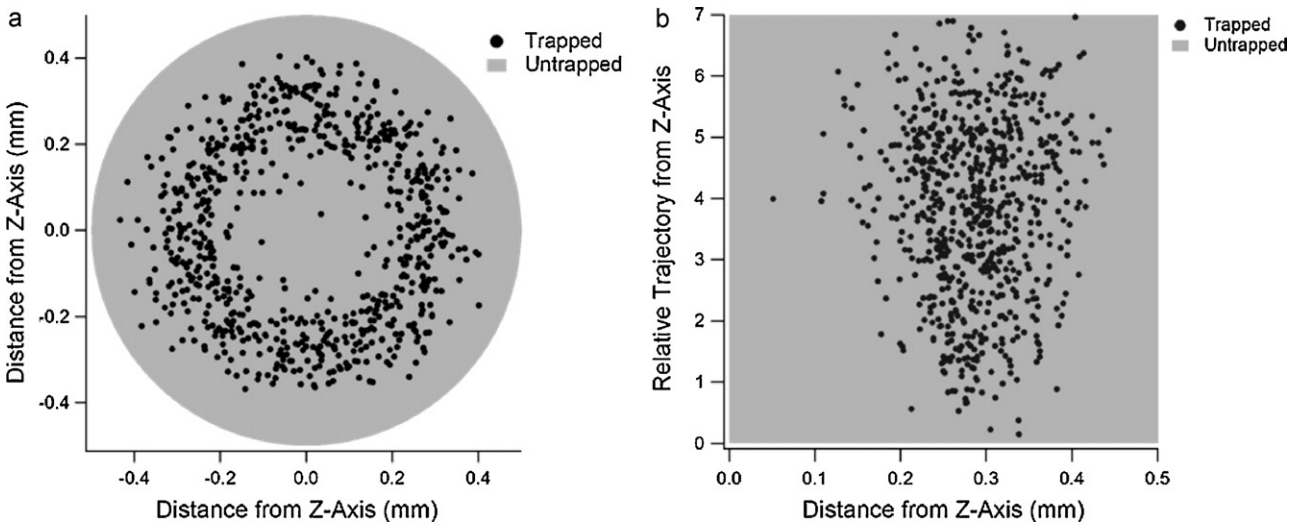

Fig. 4. For the "old" design: (a) starting positions of trapped particles as they exit the DIG and enter into the SIMION simulation and (b) starting trajectories and distance from the *Z*-axis of trapped particles. For this simulation, 0.052% of the particles were trapped.

of values; that is particles are less limited in their starting kinetic energies. Given a nominal particle TOB, there are several subsets of energies which can be trapped. In practice, these characteristics are advantageous since the range of kinetic energies that can be trapped is larger in relation to the magnitude of the kinetic energy and changes less over the trap cycle.

Fig. 6 shows the starting conditions (position and trajectory) for the new design. When compared with similar plots in Fig. 4, the new design is shown to encompass a wider range of starting parameters that permit trapping. Specifically, particles can be trapped across the full range of starting positions even though the DIG aperture is wider (Fig. 6a). The larger orifice diameter of the new design provides a 4× increase in the area of the particle beam exiting the DIG and potentially corresponds to a 4× increase in the number of particles allowed to enter the DIT and be trapped.

Another benefit of the new design is a larger transmission efficiency of particles from the DIG to the DIT. The transmission efficiency is defined as the fraction of particles having the correct kinetic energy (but differing starting position, trajectory and TOB) that are able to pass from the DIG to the DIT. For the distribution of starting conditions used in the simulation, about twice as many particles become trapped with the new design (Figs. 4 and 6). This increase in the simulated trapping efficiency should correspond to an additional 2× increase in the number of particles trapped beyond the increase discussed above for the larger DIG aperture.

When taken together, these simulations suggest that the new design should provide almost an order of magnitude increase in the number of particles trapped. A limitation of the simulations is the inability of SIMION to model particle motion through the aerodynamic lens and DIG, which determines the actual range of starting conditions for particle trapping in the DIT. For this reason, quantification of performance of the new design is made through experimental measurements. These measurements are presented in the following sections.

3.2.2. *Particle trapping as a function of particle size*

An important feature of the new design is that a single set of conditions traps a wider range of particle sizes than the old design.

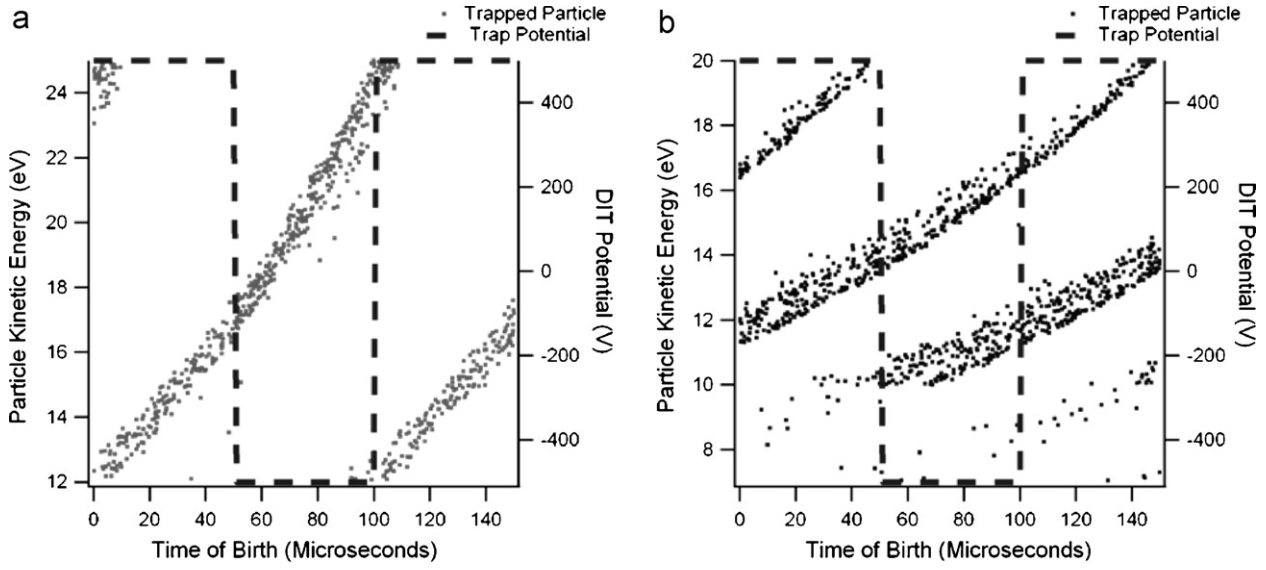

Fig. 5. Initial kinetic energy (eV) of 25 nm dia. trapped particles as a function of TOB: (a) old design and (b) new design. In each simulation, the ring electrode frequency is 10 kHz and the FAL voltage is −500 V. The dashed line indicates the ring electrode potential at each time point.

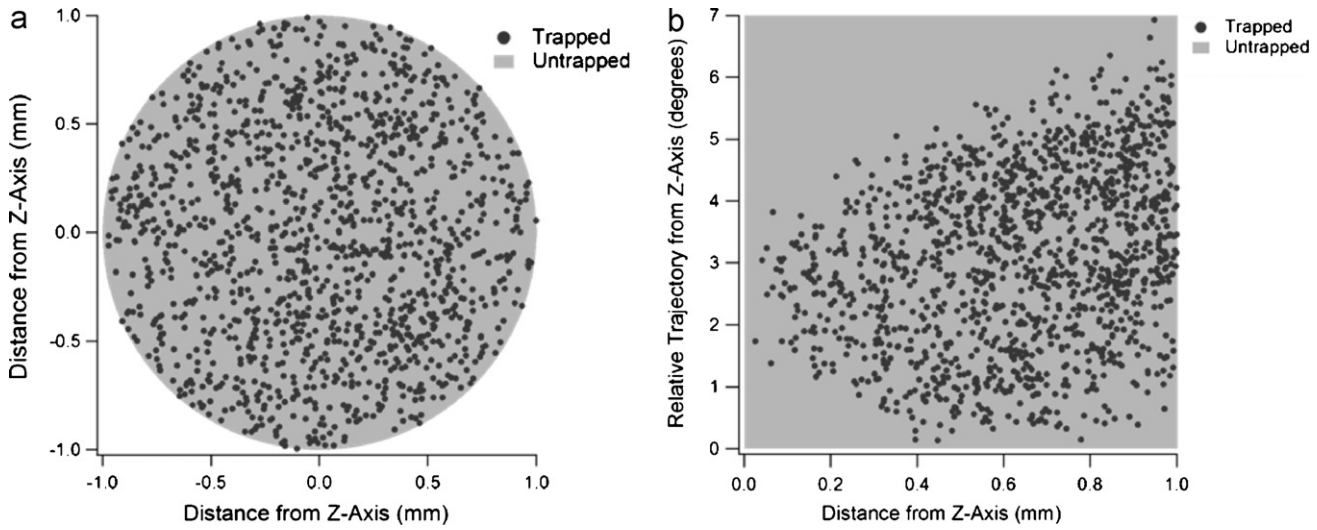

Fig. 6. For the "new" design: (a) starting positions of trapped particles as they exit the DIG and enter into the SIMION simulation and (b) starting trajectories and distance from the *Z*-axis of trapped particles. For this simulation, 0.099% of the particles were trapped.

This feature is illustrated in Fig. 7a where the measured detection efficiency (fraction of particles sampled into the NAMS that give a detected atomic ion current in the TOF analyzer) is plotted vs. mass normalized diameter for both configurations using the same set of conditions: FAL = −500 V, ring electrode frequency = 10 Hz. In this experiment, the SMPS was used to select various mobility diameters of sucrose particles; however Fig. 7a is plotted as a function of mass normalized diameter using Eq. (1). It is important to note that the experimental parameters (trap frequency, FAL voltage, pressures) chosen for Fig. 7a were those that worked best for the old design (mass normalized diameter of 25 nm) and were not necessarily optimized for the new design.

In Fig. 7a, the detection efficiency (defined as the fraction of particles entering the NAMS inlet that is subsequently analyzed) is plotted vs. mass normalized diameter. The plots are similar for the two designs at small particle sizes, which is to be expected because the design change should have no effect on the high q_z cutoff for stable motion in the trap (Eq. (2)). The plots differ substantially at large particle sizes, with the new design extending to much larger sizes. The reason for this difference can be understood based on Eq. (4). The new design traps lower kinetic energy particles than the old design (Fig. 3a). This means that large particles, which have intrinsically higher kinetic energies exiting the DIG than small particles, are better able to meet the trapping criterion in Eq. (4) with the new design in part because the longer DIG yields lower particle kinetic energies. The extended particle size range of the new design is potentially quite useful for ambient measurements of polydisperse aerosol since a wider range of particle diameters is trapped, and therefore a greater number of particles will be analyzed when the particle concentration is low. This is important because when the particle concentration is low, the number of particles analyzed is also low and there is a large uncertainty in the measured chemical

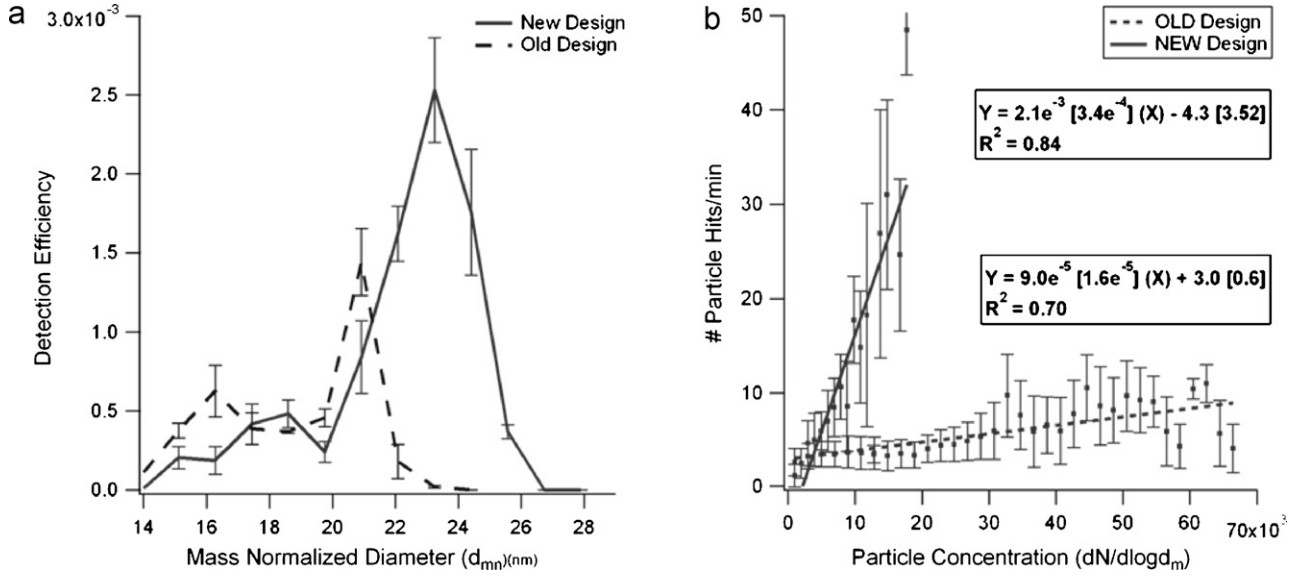

Fig. 7. (a) Experimental measurement of the detection efficiency of size selected aerosol at a single set of instrumental parameters for the (i) "old" and (ii) "new" designs. (b) Plot of ambient aerosol concentration measured with SMPS ($dN/d\log d_m$) vs. NAMS hit rate (particles analyzed per minute) for representative three day periods in (i) Pasadena, California using the old design and (ii) Hyytiälä, Finland using the new design. The values in brackets indicate standard deviations for the slope and intercept. For both measurements, FAL = −500 V, ring electrode frequency = 10 kHz, ring electrode potential = −507 V/+504 V. For the Hyytiälä, the Einzel lens potential was −25 V.

composition. The wider size range of the new design combined with its improved transmission and trapping characteristics should permit many more particles to be analyzed in a given time period and thereby reduce the measurement uncertainty.

3.3. Improved performance for ambient particle analysis

To show the effect of the new design on particle analysis, NAMS data from two measurement campaigns are compared. These campaigns represent the last use of the "old" NAMS design (Pasadena, California in spring 2010) and the first use the "new" NAMS design (Hyytiälä, Finland in spring 2011). For these two campaigns, the NAMS hit rate (defined as particles analyzed in a 1-min time period) is plotted vs. the aerosol concentration measured with SMPS ($dN/d\log d_m$) averaged over the appropriate mobility diameter range (nominally 20–25 nm) for the same 1-min time period. Fig. 7b shows the combined results for three representative days during each campaign. Each dataset is fit by a linear regression to give the analysis rate (defined as the slope of the regression line) for the corresponding NAMS configuration. The new configuration is found to give a 23-fold increase in analysis rate. The individual data points vary widely (especially at low particle concentrations) and there are several reasons for this variation. (1) SMPS measures mobility diameter while NAMS traps particles based on mass-normalized diameter. If the particle composition changes significantly from one time period to the next, then the corresponding density change will alter the relationship between the two measurements (Eq. (1)). (2) Poorly controlled conditions inside the instrument trailer such as temperature and mechanical vibration can cause laser position to be altered slightly, changing the NAMS hit rate. (3) The uncertainty associated with counting statistics is significant when a small number of particles is analyzed in a given time period. (4) The total particle concentration in Pasadena (integrated over all sizes) was so large that the hit rate included a background contribution from untrapped particles that were randomly hit as they passed through the DIT. Despite these complications, Fig. 7b clearly shows the benefit of the new design. The increase in analysis rate is especially useful when performing ambient particle analysis in a remote location such as Hyytiälä where the aerosol concentrations are more than an order of magnitude lower than in an urban environment such as Pasadena.

4. Conclusions

Nanoparticles acquire a significant amount of kinetic energy when they move from atmospheric pressure into the vacuum of a mass spectrometer. If a particle is to meet the kinetic energy criterion for trapping, then much of this energy must be removed. Injecting a charged particle into the trap requires the insertion of a field adjusting lens (FAL) upstream of the trap. The particle kinetic energy and FAL voltage required for trapping are strongly correlated with each other, and their magnitudes are strongly dependent on the design of the FAL assembly. The particle transmission efficiency into the trap and the size range of particles able to be trapped with a single set of conditions both can be maximized with a proper design of the FAL assembly. An optimized FAL design has been incorporated into the nano aerosol mass spectrometer (NAMS) which is shown to increase the particle analysis rate by over an order of magnitude. With the new NAMS design, an ambient aerosol concentration ($dN/d\log d_m$) of 1×10^3 will yield approximately 2–3 particles analyzed per minute.

Acknowledgements

This research was supported by the National Science Foundation grant number CHE0808972. Ambient measurements in Hyytiälä, Finland were performed with logistical and financial assistance from M. Kulmala and D. Worsnop at the University of Helsinki.

References

[1] B.V. Bhaskar, V.M. Mehta, Atmospheric particulate pollutants and their relationship with meteorology in Ahmedabad, Aerosol and Air Quality Research 10 (2010) 301–315.
[2] J.J. de Hartog, G. Hoek, A. Mirme, T. Tuch, G.P.A. Kos, H.M. ten Brink, B. Brunekreef, J. Cyrys, J. Heinrich, M. Pitz, T. Lanki, M. Vallius, J. Pekkanen, W.G. Kreyling, Relationship between different size classes of particulate matter and meteorology in three European cities, Journal of Environmental Monitoring 7 (2005) 302–310.
[3] S. Qu, E.N. Liberda, Q.S. Qu, L.C. Chen, In vitro assessment of the inflammatory response of respiratory endothelial cells exposed to particulate matter, Journal of Toxicology and Environmental Health. Part A: Current Issues 73 (2010) 1113–1121.
[4] J. Boczkowski, P. Hoet, What's new in nanotoxicology? Implications for public health from a brief review of the 2008 literature, Nanotoxicology 4 (2010) 1–14.
[5] A. Nel, T. Xia, L. Madler, N. Li, Toxic potential of materials at the nanolevel, Science 311 (2006) 622–627.
[6] C.C. Lin, K.L. Huang, S.J. Chen, S.C. Liu, J.H. Tsai, Y.C. Lin, W.Y. Lin, NH^{4+}, NO^{3-}, and SO_4^{2-} in roadside and rural size-resolved particles and transformation of NO_2/SO_2 to nanoparticle-bound NO_3/SO_4^2, Atmospheric Environment 43 (2009) 2731–2736.
[7] B.R. Bzdek, M.V. Johnston, New particle formation and growth in the troposphere, Analytical Chemistry 82 (2010) 7871–7878.
[8] S.Y. Wang, C.A. Zordan, M.V. Johnston, Chemical characterization of individual, airborne sub-10-nm particles and molecules, Analytical Chemistry 78 (2006) 1750–1754.
[9] S.Y. Wang, M.V. Johnston, Airborne nanoparticle characterization with a digital ion trap-reflectron time of flight mass spectrometer, International Journal of Mass Spectrometry 258 (2006) 50–57.
[10] C.A. Zordan, S. Wang, M.V. Johnston, Time-resolved chemical composition of individual nanoparticles in urban air, Environmental Science and Technology 42 (2008) 6631–6636.
[11] J.P. Klems, M.R. Pennington, C.A. Zordan, L. McFadden, M.V. Johnston, Apportionment of motor vehicle emissions from fast changes in number concentration and chemical composition of ultrafine particles near a roadway intersection, Environmental Science and Technology (2011).
[12] B.R. Bzdek, C.A. Zordan, G.W. Luther, M.V. Johnston, Nanoparticle chemical composition during new particle formation, Aerosol Science and Technology 45 (2011) 1041–1048.
[13] C.A. Zordan, M.R. Pennington, M.V. Johnston, Elemental composition of nanoparticles with the nano aerosol mass spectrometer, Analytical Chemistry 82 (2010) 8034–8038.
[14] C. Ma, H.W. Lee, D.M. Lubman, Computer-simulation of the operation of a 3-dimensional quadrupole ion trap, Applied Spectroscopy 46 (1992) 1769–1779.
[15] S. Dobashi, Y. Deguchi, N. Fukuda, M. Kira, R. Tanaka, Y. Izawa, T. Kubota, On-line monitoring method of PCBs by laser ionization dynamic trapping time of flight mass spectrometry, Bunseki Kagaku 53 (2004) 1441–1448.
[16] G.A. Salazar, T. Masujima, Computer simulation of the gap-tripole ion trap with linear injection, 3D ion accumulation, and versatile packet ejection, Journal of the American Society for Mass Spectrometry 19 (2008) 1367–1374.
[17] C.L. Hendrickson, S.C. Beu, G.T. Blakney, A.G. Marshall, SIMION modeling of ion image charge detection in Fourier transform ion cyclotron resonance mass spectrometry, International Journal of Mass Spectrometry 283 (2009) 100–104.
[18] L. Ding, M. Sudakov, S. Kumashiro, A simulation study of the digital ion trap mass spectrometer, International Journal of Mass Spectrometry 221 (2002) 117–138.
[19] D.-R. Chen, D.Y.H. Pui, A high efficiency, high throughput unipolar aerosol charger for nanoparticles, Journal of Nanoparticle Research 1 (1999) 115–126.
[20] A. Held, G.J. Rathbone, J.N. Smith, A thermal desorption chemical ionization ion trap mass spectrometer for the chemical characterization of ultrafine aerosol particles, Aerosol Science and Technology 43 (2009) 264–272.
[21] D. Manura, http://www.simion.com/info/Collision_Model_HS1 (last accessed June 2011).
[22] X.L. Wang, F.E. Kruis, P.H. McMurry, Aerodynamic focusing of nanoparticles. I. Guidelines for designing aerodynamic lenses for nanoparticles, Aerosol Science and Technology 39 (2005) 611–623.
[23] X.L. Wang, A. Gidwani, S.L. Girshick, P.H. McMurry, Aerodynamic focusing of nanoparticles. II. Numerical simulation of particle motion through aerodynamic lenses, Aerosol Science and Technology 39 (2005) 624–636.
[24] R.E. March, An introduction to quadrupole ion trap mass spectrometry, Journal of Mass Spectrometry 32 (1997) 351–369.